VOL. 5, NO. 5, MAY 2010 ISSN 1819-6608
ARPN Journal of Engineering and Applied Sciences


www.arpnjournals.com

IMPLICITY DYNAMIC SIMULATION OF CONTACT BEHAVIOUR OF THE QUASI-ISOTROPIC CARBON FIBROUS COMPOSITE PANELS

Umar Farooq and Karl Grehory
Built Environment and Engineering Department, University of Bolton, United Kingdom
E-Mail: uf1res@bolton.ac.uk, k.r.gregory@bolton.ac.uk

ABSTRACT

In this paper computational modeling and simulation of the contact response of the quasi- isotropic carbon fibrous composite panels against blunt nose tip indenters has been studied. Mathematical modeling of spatial contact interaction was developed and incorporated into the finite element analysis software ABAQUS™ using implicit dynamic integration routine. Effect of ply orientation, thickness, indenter size, and variable loads were studied. Both the isotropic and quasi-isotropic material models were simulated. The comparison of computer generated stresses, strains and deflections show that laminate thickness, material properties, loads and indenter sizes have significant affect on individual plies. The approach significantly reduces complexity in modeling some of the similar problems. The obtained results could be useful in improving the simulation modeling for design parameters. The selected results are included in the forms of graphs, contour plots and legend tables.

Keywords: finite element analysis, fibrous composites laminates, contact behaviour, stress analysis.

1. INTRODUCTION

Analysis and prediction of materials' contact response when subjected to transverse loading finds applications in low velocity impacts, flexural tests for material characterizations. The contact studies also have applications in tribology, three- and four-point bending tests for flexural, shear strength of materials. Some of the other applications are ball and roller bearing, locomotive wheels, host of machine components, parts of machines, plain bearings, hinges, and other applications of engineering mechanics. Several studies of the contact between indenters and plates have been published some of them are given below:

The stress state using Hertz theory in a narrow set of the contact problem was studied in (Shaterman, 1949). The fibre orientation relative to the sliding direction in the contact behaviour of fibrous plastic-metal where couples becoming less significant as the fibre volume fraction increases predicted in (Giltrow, 1970). Sun in (Sun and Tang, 1982-1985) performed static indentation test to investigate low-velocity impact phenomena of composite laminates. Ccontact behaviour of orthotropic beams was investigated in (Keer, 1986). Wu *et al*., in (Wu, 1993) studied the contact between a composite laminate and a cylindrical indenter. An analysis of the indentation of simply supported laminated plates under rigid spheres using three-dimensional elasticity theory indicated that the stacking sequence has little effect on the contact law confirming previous experimental results (Wu and Yen, 1994). Many researchers studied the low-velocity impact problem on composite laminates following the 'lumped mass method' to approximately calculate contact force history of composite laminates subjected to low-velocity impact as reported in (Hong and Choi, 1994). Analytical models of elastic contact of system of finite cylindrical bodies are widely used in applications of engineering mechanics for calculating a stress state of some parts of machines, such as plain bearings, hinges. It forms a base for calculating a stress state of some parts of machines, such as plain bearings, hinges as studied in (Kovalenko, 1995). However, analytical methods such as complex potential theory can't be used in many cases due to the bulky character of mathematical transformations (Kovalenko, 1995; Chernets, 1996). Aanalytically and experimentally investigation on contact to study low-velocity impact problems of composite laminated structures were listed in (Abrate, 2001). The initial softness allowances of metals to deform and fill voids among asperities at the contact surface were studied in (A-Al-Mayah, 2003) indicating that sandblasting the inner surface of the metal counterpart further increased the shear stress. The 'spring element method' to analyze impact response of composite laminates using spring or gap element solved using general purpose commercial FEM software (Lim and Choi, 2004). Impact characterisation of low fibre-volume glass reinforced polyester circular plates were studied by Sutherland in (Sutherland, 2005). The effect of sleeve material contact and hardness on the interfacial grip was considered experimentally using copper and aluminium alloy for carbon fibrous plastics rod was studied in (A-AL-Mayah, 2006). Predictions of stresses in transversely isotropic composite plates were studied by Robin in (Robin and Soren, 2006). Finite element modelling of composite plates with internal delamination due to contact was studied Alnefaie in (Alnefaie, 2009). Finite element modelling and simulation model was developed by Farooq in (Farooq, 2009) to study the contact interaction and deformation of carbon fibrous composite beam against rigid indenters.

Several software programs have been developed to analyze stress state of interacting bodies. However, certain difficulties arise when these programs solve three-dimensional contact problems if local geometric peculiarities, high cost of software and the required equipment are taken into account. Moreover, existing investigations can't be used in many cases of contact

interaction due to the bulky character of mathematical transformation. The case of aligned fibrous composites as the contact law becomes much more complex because of the contacting lamina and their sequences are additional parameters. These issues need to be adequately addressed by developing simulation models.

The present approach has addressed the important issue of modeling complex contact problems into simple and easy implicit dynamic routine, which could be reproduced, extended and re-run for number of similar problems. Computer generated results could be utilized to study damage, fatigue, and failure predictions required for design improvements.

2. MATHEMATICAL FORMULATION OF HERTZ CONTACT FOR LAMINATED COMPOSITES

The first step towards the solutions of contact problems is the determination of the size and shape of the contact area as well as the distribution of normal pressure acting on the area. Geometrical effects on local elastic deformation properties have been considered as early as 1880 with the Hertzian theory (Timoshenko, 1951). The Hertz theory relates stresses owing to the contact of a sphere on a plane, a sphere on a sphere, a cylinder on a cylinder, etc. The application of a load over a small area of contact results in usually high pressures. Situations of such nature are found on a small microscopic scale whenever force transmitted through bodies in contact. The stresses and deformations resulting from the interfacial pressure are then evaluated.

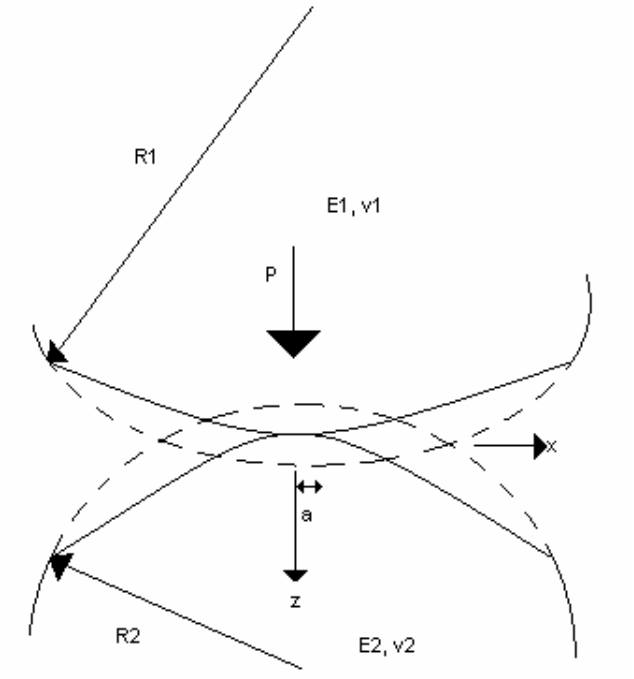

Figure-1. Two surfaces in contact.

In Figure-1, P is the pressure one surface applies to the other. R_1, E_1, and v_1 and R_2, E_2, and v_2 are the radius, Young's Modulus, and Poisson's ratio of surfaces 1 and 2 respectively and 'a' is one half the length of the contact patch, which is defined by the other variables. Hertz supposed that for the calculation of local stresses each body may be considered as an elastic half-space loaded along a small elliptical area on its surface. In order to define 'a', the characteristic radius 'R' must first be defined as

$$\frac{1}{R} = \frac{1}{R_1} + \frac{1}{R_2} \tag{1}$$

Next an equivalent Young's modulus must be defined

$$\frac{1}{E} = \frac{1}{E_1} + \frac{1}{E_2};$$

$$\frac{1}{E^*} = \frac{(1-v_1^2)}{E_1} + \frac{(1-v_2^2)}{E_2} \tag{2}$$

Where E* is the equivalent Young's modulus. The area "a" can then be defined as "$a = \sqrt{\frac{PR}{E^*}}$". Next the pressure along the contact patch reduces to

$$p(x) = \left(\frac{PE^*}{\pi R}\right)^{\frac{1}{2}} \left[1 - \left(\frac{x}{a}\right)^2\right]^{\frac{1}{2}} \text{ or}$$

$$P(r) = P_0 \left(1 - \frac{r^2}{a^2}\right)^{1/2} \tag{3}$$

The way stress was calculated for general load on an elastic half space but using 'a' as one half the length of the contact area, zero for all applied sheet stresses and p(x) for the pressure along the contact area. The static indentation of laminated composites includes the unloading and reloading phases. During the first loading phase, the contact law closely follows Hertz's law of contact:

$$P = k\alpha^{\frac{3}{2}} \tag{4}$$

The radius of the indenter and the elastic properties of the impactor and the target can be found using

$$k = \frac{4}{3} E R^{\frac{1}{2}} \tag{5}$$

With R given by Eq.(1) and E is given by Eq.(2), E_2 being the transverse modulus of the composite. Poisson's ratios of the composite were neglected. Since Hertz's contact law is for semi-infinite solids, this modified law includes the effect of the properties of the target on the contact behaviour through only the out-of-plane stiffness (modulus E_3) of that ply of the target which comes into contact with the impactor. A modified form of the Hertz contact law is used to study composites. The

contact law should depend on the thickness of plies, the relative orientation of various plies and various stiffness constants.

$$P = P_m \left[\frac{(\alpha - \alpha_0)}{(\alpha_m - \alpha_0)} \right]^{2.5} \quad (6)$$

Equation (7) describes the contact law during the loading phase of the indentation process. During the unloading phase, P_m is the maximum force reached before unloading, α_m is the maximum indentation, and α_0 is the permanent indentation, which is zero when the maximum indentation remains below a critical value α_{cr}. When $\alpha_m > \alpha_{cr}$,

$$\alpha_0 = \alpha_m \left[1 - \left(\frac{\alpha_{cr}}{\alpha_m} \right)^{\frac{2}{5}} \right] \quad (7)$$

During subsequent reloading, the resulting curve is distinct from the unloading curve but always returns to the point where unloading began. The unloading curve is modeled by

$$P = P_m \left[\frac{(\alpha - \alpha_0)}{(\alpha_m - \alpha_0)} \right]^{\frac{3}{2}} \quad (8)$$

The parameter α_0 does not necessarily correspond to the permanent indentation of the laminate, even if P = 0 when $\alpha = \alpha_0$, selected so that Eq. (8) fits the experimental unloading curve using a least squares fir procedure. The parameter α_0 is related to the actual permanent indentation α_p and the maximum indentation α_m during the loading phase by

$$\alpha_0 = \beta(\alpha_m - \alpha_p) \quad (9)$$

When $\alpha_m > \alpha_{cr}$, $\alpha_0 = 0$ otherwise. The permanent indentation α_p and the parameter β are determined from experiments. During the unloading phase the behaviour is modeled by

$$P = P_m \left[\frac{(\alpha - \alpha_0)}{(\alpha_m - \alpha_0)} \right]^{q} \quad (10)$$

Where the permanent indentation α_0 was the maximum load P_m and the present exponent q has an average value of 4.1. The exponent in Eq. (11) compared to 1.5 for Herzian contact, and that q = 4.1 for this Kevlar-epoxy laminate for glass-epoxy and graphite epoxy the usual value is 2.5. In the special case of a sphere contacting a body of the same material but having a flat surface, the equations lead to the contact pressure distributed over a small circle of radius 'a' given by

$$a = 0.88\left(\frac{2Pr_1}{E}\right)^{\frac{1}{3}} \quad \sigma_c = 0.62\left(\frac{PE^2}{4r_1^2}\right)^{\frac{1}{3}} \quad e = 1.54\left(\frac{P^2}{2E^2 r_1}\right)^{\frac{1}{3}} \quad (11)$$

3. COMPUTATIONAL PROCEDURE OF IMPLICIT TIME INTEGRATION

Computational contact procedure was developed on the basics of non-linear continuum mechanics employing numerical methods such as the finite element method. The contact was considered as a boundary condition. The process of solving the equilibrium condition is equivalent to the minimisation of total potential energy of the system in terms of the prescribed displacement field extended to a variational formulation.

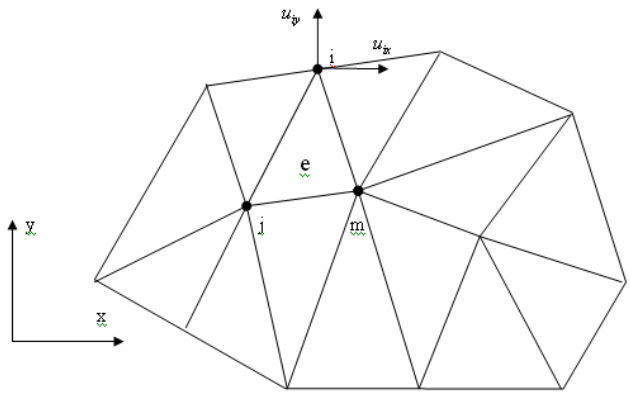

Figure-2. 2D discrete plane with triangular elements.

In Figure-2, a typical finite element, e, is defined by nodes, i, j, m and straight line boundaries, N is force, B is differential and D is the elastic matrices. By imposing a virtual nodal displacement du, equilibrium with the external and internal work is achieved. The work done by the nodal forces is the sum of the products of the individual force component and the corresponding displacement in which f is the body force. Employing the virtual work principle that equates the external work to the total internal work, Eq. (12) is obtained:

$$F_e = (du_e) \int (B^T DB\sigma \, dx \, dy) u_e - \int Nf \, dx \, dy \quad (12)$$

Substituting Eqs. (12), the following equation can be obtained:

$$(du_e) F_e = (du_e)\left(\int B\sigma \, dx \, dy - \int Nf \, dx \, dy \right) \quad (13)$$

wher $k_e = \int (B^T DB\sigma \, dx \, dy)$ is the matrix of element stiffness. Fe is a set of unknown parameters. In order to determine the displacement field ue, boundary conditions must be employed to resolve these equations at the overall system level. The stiffness of the whole system is obtained

by assembling the stiffness matrices of all elements together.

$$K = \sum k^e \tag{14}$$

The principle of virtual displacement used above ensures the equilibrium of the system for the displacement pattern that minimises the potential energy. The equilibrium would be complete only if the virtual work equality for all arbitrary variations of displacement were ensured. Balancing the internal energy with the external work:

$$\int (d\,\varepsilon)\sigma\, dV + \left[\int (d\,u)\, f\, dV + \int (d\,u)\, f_b\, dS\right] = 0 \tag{15}$$

The first term of the above equation be recognized as the variation of the strain energy of the structure, and the second term that is in the brackets is the variation of the potential energy of external loads. Rewriting Eq. (15):

$$d\left(\Pi_{\text{int}} + \Pi_{ext}\right) = d\left(\Pi_p\right) = 0 \tag{16}$$

is the total potential energy. This means the finite element method seeks a displacement field that keeps the total potential energy stationary and minimised. In that case, finite element method can be used in any problem in which function could be specified or in the following minimum condition:

$$\frac{\partial \Pi_p}{\partial u} = \begin{Bmatrix} \dfrac{\partial \Pi_p}{\partial u_1} \\ \dfrac{\partial \Pi_p}{\partial u_2} \\ . \\ . \\ . \end{Bmatrix} \tag{17}$$

The displacement field can be obtained, and other terms such as the strain and the force are derived from the obtained displacement. However, because of the material plasticity and contact boundary condition, the non-linearity is involved. Thus the approach is generalized to accommodate the nonlinear problems. The governing equations are written in the general form as:

$H(u) = \begin{Bmatrix} H_1(u) \\ H_2(u) \\ . \\ . \\ . \end{Bmatrix} = 0$, In the domain with the boundary conditions $J(u) = \begin{Bmatrix} J_1(u) \\ J_2(u) \\ . \\ . \\ . \end{Bmatrix} = 0$

The equivalent weak-form is expressed as

$$\int w\, H(u)\, d\Omega + \int \overline{w}\, J(u)\, d\Gamma = 0 \tag{18}$$

Where w and w are arbitrary parameters called weighted coefficient, with lower requirement of connectivity for displacement function. The solution in approximation form is written as following:

$$u = \sum N_i\, d_i = Nd \tag{19}$$

Where d is the nodal displacement field. The approximation is written as:

$$\int w\, H(N\,d)\, d\Omega + \int \overline{w}\, J(N\,d)\, d\Gamma = 0 \tag{20}$$

The H (Nd) and J (Nd) represent the residual obtained by substitution of the approximation into the differential governing equations. The method chooses the shape function as the weighted coefficient and written as $W_j = N_j$. As a result, the Eq. (21) is derived:

$$\int N\, H(N\,d)\, d\Omega + \int N\, J(N\,d)\, d\Gamma = 0 \tag{21}$$

The contact pressure and traction represented by term f_b are considered as boundary constraints. The Lagrange multiplier method and the Penalty method of contact constraint enforcement are employed to solve the equilibrium equations. Contact is a complex boundary condition because of its nonlinearity. Before employing the contact constraint enforcement to solve the equilibrium equations, the relation between contact pressure/traction and displacement was set up. As the state of contact affects the relationship between the contact pressure/traction and the displacement, first the computational approach should establish the occurrence of contact. The following conditions are required to be assessed in each computational step.

$$\begin{cases} non - coontact \\ contact \begin{cases} stick \\ slip \end{cases} \end{cases}$$

A potential algorithm is presented as a simple illustration. Consider Figure-3 indicating two elastic bodies Bi, x i denotes coordinates of the original configuration. In the normal direction of contact, non-penetration condition is defined as gap function N $_g$ given by:

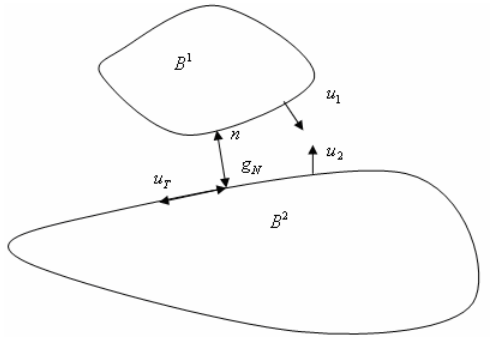

Figure-3. Two bodies in contact.

$$g_N = g_{N_0} - (u_1 - u_0).n$$
$$x \begin{cases} > & 0 & (non-contact) \\ = & 0 & contact \\ < & 0 & penetration \end{cases} \quad (22)$$

Eq. (22) is used to judge the state of contact/non-contact, in which n is the normal vector to the contact surface, g_{No} is the original gap, expressed as (23):

$$g_{N_0} = (x_2 - x_1).n \quad (23)$$

In Eq. (22), the contacting bodies penetrate into each other and the penetration is defined as g_N. The tangential motions of contact state are associated with stick and slip. Stick refers to no relative motion between the two contact bodies while slip refers to existence of relative tangential motion. The motion can be defined using a functional u_T in the tangential direction. For stick condition:

$$u_T = [I - n x n](u_1 - u_2) = 0 \quad (24)$$

While in slip conditions:

$$u_T = [I - n x n](u_1 - u_2) \neq 0 \quad (25)$$

Where I is the unit matrix. Through (22) to (25), the contact states are determined. The compressive contact pressure p within the contact patch can be expressed as:

$$P = n.\bar{\sigma}.n = 0 \quad (26)$$

Where the boundary value of stress on the contact surface. For the slip zone, the frictional tangential traction employs Coulomb friction law the stick zone, the frictional traction is expressed as:

$$q = \bar{\sigma}.n - pn \quad (27)$$

The stresses are converted to displacement based on the elastic or elasto-plastic material model. Thus, the relation between contact pressure/traction and displacement is developed. To solve the equilibrium equations, the contribution of total potential energy from the contact boundary is extracted and Eq. (17) is rewritten as:

$$\delta \Pi_p = \delta(\Pi_{ext,\text{int}} + \Pi_c) = 0 \quad (28)$$

Where sum of internal and external energies except from the boundary of contact is the energy contribution from contact. The further extended as:

$$\Pi_{ext,\text{int}} = \int \{\varepsilon\}^T \{\sigma\} dv + \{\ddot{u}\}^T \{m\}\{u\} dv + \int \{f\}\{u\} dv + \int \{u\}^T \{f_b\} dS \quad (29)$$

One of the most widely applied implicit methods is the Newmark in (Newmark, 1959) method. The approximation of displacement and velocity are based on the following two functions:

$$u_{n+1} = u_n + \Delta t \dot{u}_n + \frac{(\Delta t)^2}{2}[(1-2\nu)\ddot{u}_n + 2\nu \ddot{u}_{n+1}] \quad \dot{u}_{n+1} = \dot{u}_n + \Delta t[(1-\vartheta)\ddot{u}_n + 2\vartheta \ddot{u}_{n+1}] \quad (30)$$

Where the constant parameters an be chosen freely and the order and accuracy of the method is determined. By inserting Eq. (17) into Eq. (30)

$$m\ddot{u} + C_d \dot{u} + K u = F \quad (31)$$

The equilibrium equation which can be solved by using some iteration method such as Newton method. After obtaining solution for acceleration, the displacement and velocity can be worked out using Eq. (31).

The nature of contact problems determines that the time increment should be small and hence the number of increments would be numerous. By using the implicit method, the computational cost would be expensive as every increment would involve a number of iterations but procedure is easy and simple.

4. NUMERICAL RESULTS AND DISCUSSIONS

The commercially available software ABAQUS^{TM} has a good capability for studying impacted surface behaviour and offers two different methods for modeling the contact: small sliding and finite sliding formulations. The small sliding approach implemented here uses Lagrange formulation that the contacting surfaces can only undergo relatively small sliding relative to each other, but arbitrary rotation of the bodies is permitted. Here, of the two contacting surfaces, the indenter (the slave) is rigid. The nodes of the slave surface

are constrained not to penetrate into the master surface. Consequently, the contact direction is always normal to the master surface. The contact between the surfaces is hard contact, i.e. when the surfaces are in contact any pressure stress can be transmitted between surfaces with no penetration of one surface into another. The surfaces separate if the pressure reduces to zero. By small sliding it is meant that a given slave node will interact with the same local area of the master surface during interaction. Because of such facilities the software was selected for this study. Two independent parts were created in part module of and assembled in the assembly module. Dimensions of the specimen plate are dimension 0.3048 m x 0.3048 m x 0.00288 m. The indenter block has Young's modulus of 15 GPa and Poisson's ratio of 0.3 with dimensions of 0.1524 m x 0.1524 m x 0.0762 m as indicated in the Figure-4 below.

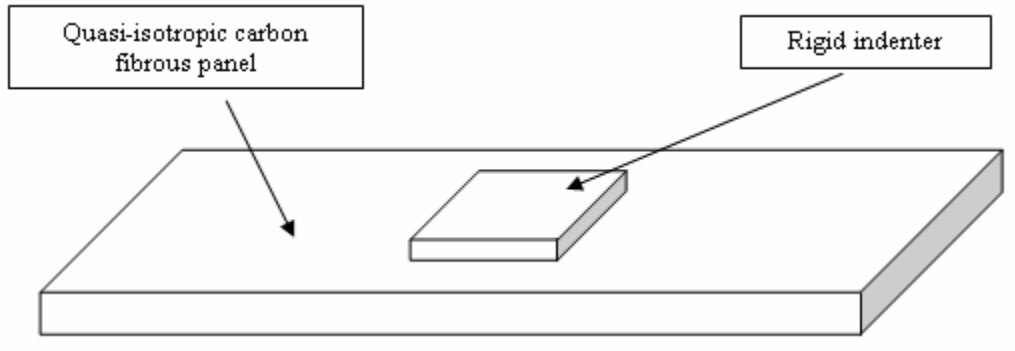

Figure-4. Schematic view of the laminated plate and the indenter in contact.

The isotropic and quasi-isotropic properties were assigned to the models and simulations were carried out for 0.11 seconds. Twenty-thousand maximum number of increments with increment size of 0.001 were introduced. Full Newton techniques were selected while half-step residual calculations were suppressed. Both the models were fully clamped and were contacted by a fully free steel block at the centre pushed by a 10 Newton load. Material properties of the isotropic specimens were used as E = 150 GPa with 0.3 Poisson's ratio, the properties of the quasi-isotropic specimens of 8-ply are given in the Table-1 below:

Table-1. Laminate of stacking sequences $[45/0/-45/90]_S$.

Material properties	**Ultimate strengths MPa**
$E_1 = 150$ GPa, $E_2 = E_3 = 15$ GPa	$\left(\sigma_1^T\right)_{ult} = \left(\sigma_1^C\right)_{ult} = 1500$
$G_{12} = G_{13} = 5.7$ GPa $G_{23} = 7.26$ GPa Poisson's Ratios $\nu_{12} = 0.33$ $\nu_{23} = 0.03$ $\nu_{13} = 0.01$	$\left(\sigma_2^T\right)_{ult} = 40$ $\left(\tau_{12}\right)_{ult} = 53$ $\left(\sigma_2^C\right)_{ult} = 20$

Mapped meshing options were selected to create adequate number of elements in the regions where high concentrations of deformations were expected. The meshed model is given below in Figure-5.

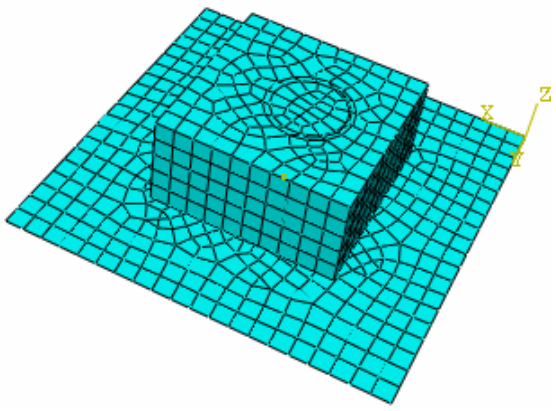

Figure-5. Computer generated meshed model.

Computer generated results were obtained and some of the selected ones are presented for comparison and discussion. Comparisons of displacement graphs shown in Figure-6 demonstrate that specimen of isotropic material behave elasto-plastically at the threshold contact load. However, the graph of the quasi-isotropic model as in shown in the same figure demonstrated a significant reduction in strength change that confirms that ply (ies) failure at that point.

Legend Tables and contour plots as shown in Figure-7 demonstrate that displacement values of quasi-isotropic material model are three times higher from the isotropic model which demonstrate further that the quasi-isotropcic model three-fold elastic than the isotropic material model. Legend Tables and contour plots for isotropic material model and ply 1 and ply 8 of the quasi-

isotropic material as shown in Figure-8 demonstrate that tensile stress values of quasi-isotropic material model are half of the isotropic model which demonstrates that the quasi-isotropic model absorbs considerable amount of energy and is under less tensile stresses. Legend Tables and contour plots for isotropic material model and ply 1 and ply 8 of the quasi-isotropic material as shown in Figure-9 demonstrate that compressive stress values of quasi-isotropic material model at ply 1 are double than that of the isotropic model and ply 8 of the same model. The stress values' differences are according to expectation and demonstrate that the top ply sustains very high compressive stresses. Legend Tables and contour plots for isotropic material model and ply 1 and ply 8 of the quasi-isotropic material as shown in Figure-10 demonstrate that in-plane shear stress values of quasi-isotropic material model at ply 1 are a quarter than that of the isotropic model and half of the ply 8 of the same model. The shear stress values' differences are according to expectation and confirm that the computed values are realist. Legend Tables and contour plots for isotropic material model and ply 1 and ply 8 of the quasi-isotropic material as shown in Figure-11 demonstrate that in-plane strain values of quasi-isotropic material model at ply 1 and ply 8 are almost the same. The predicted values confirm that the computational models are reliable.

Isotropic model	Quasi-isotropic model

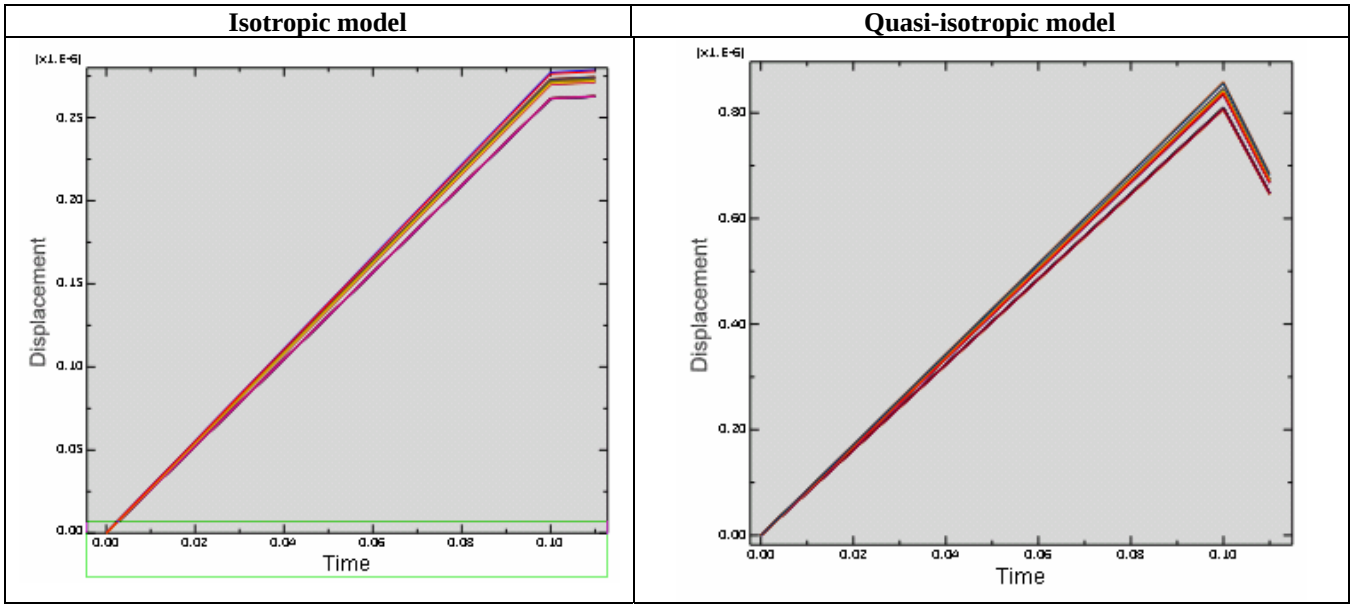

Figure-6. Graph of displacement versus time.

Isotropic model	Quasi-isotropic model

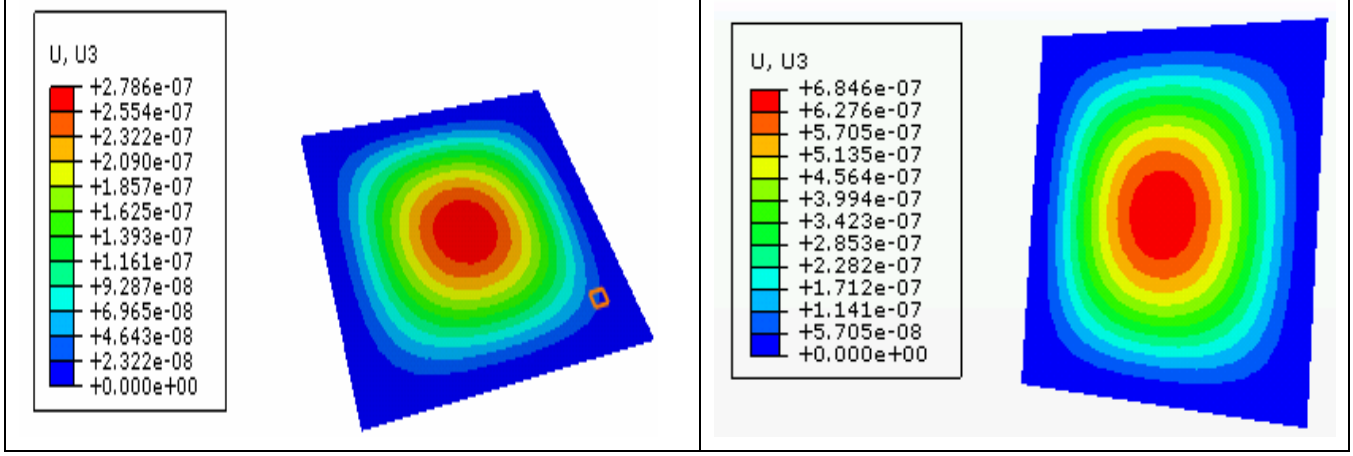

Figure-7. Legends table and contour plots of displacements.

Isotropic model	Quasi isotropic model

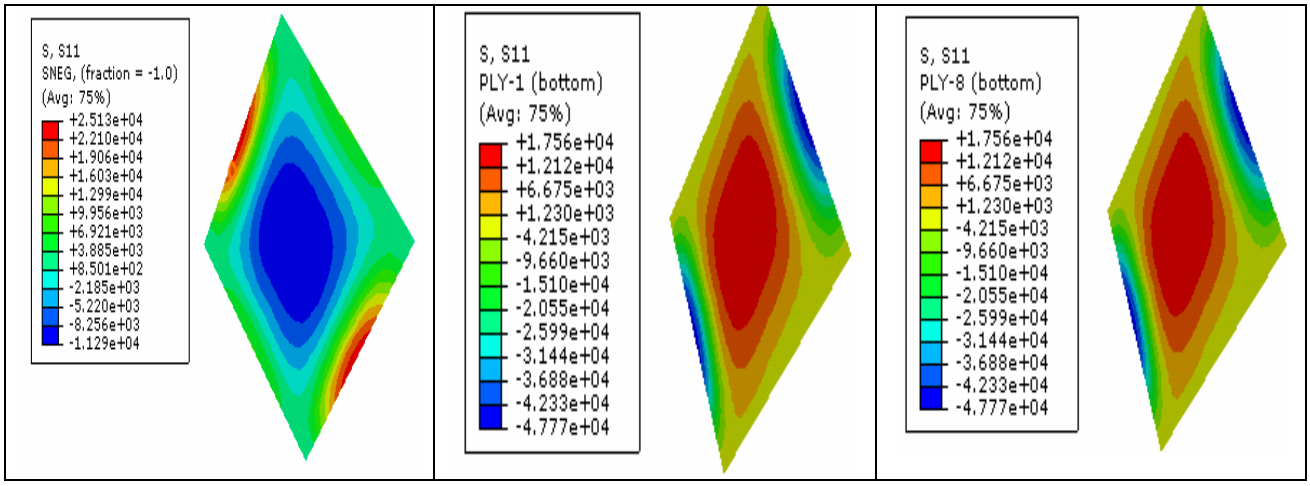

Figure-8. Legend table and contour plots of normal stresses in x-direction.

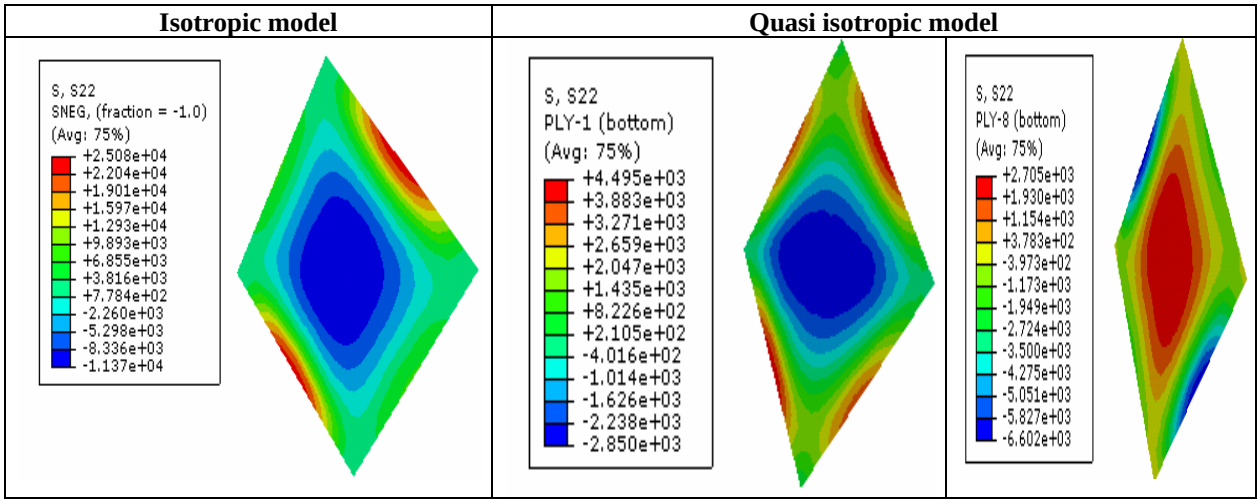

Figure-9. Legend table and contour plots of lateral normal stresses in y-direction.

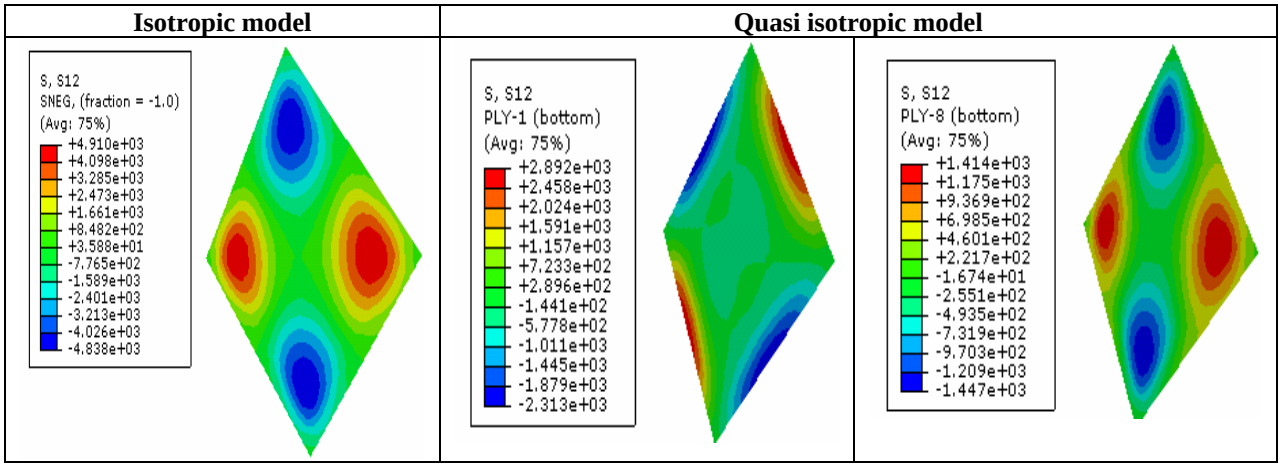

Figure-10. Legend table and contour plots of in-plane shear stresses.

Isotropic model	Quasi isotropic model

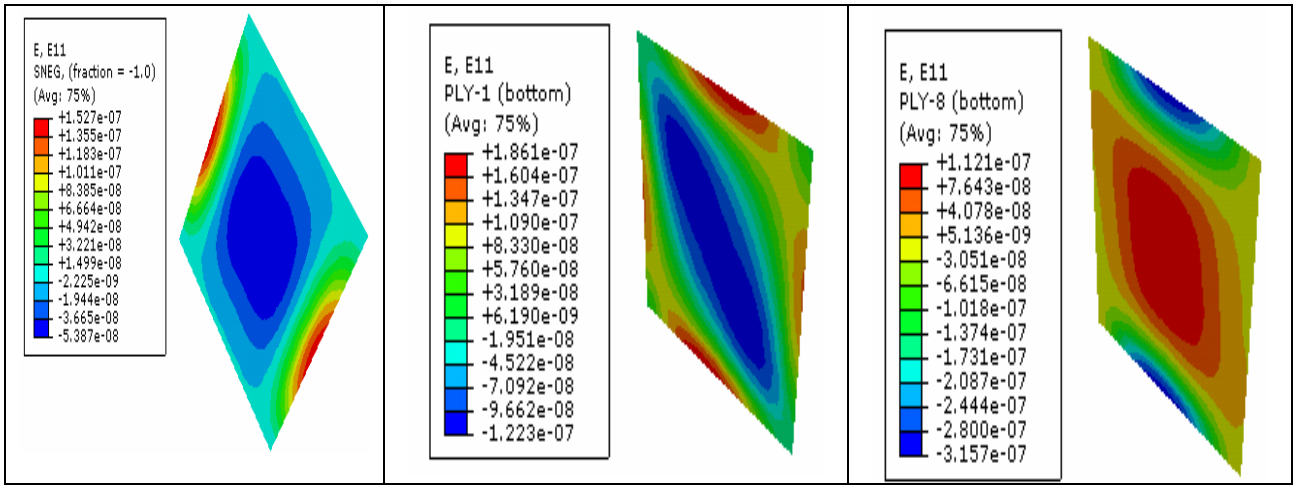

Figure-11. Legend table and contour plots of principal strains in x-direction.

The comparison of results indicated that the isotropic materials are less flexible and under less tensile strains than the quasi-isotropic material model, which means that the quasi-isotropic isotropic model is more flexible. The legend Tables and contour plots comparison indicates that the implicit dynamic model is capable to predict difference between the computed variables including strains of isotropic and quasi-isotropic models. Though the values are small yet they predict the extension incurred in the system by the contact on top plies and compression on the bottom plies. Moreover, there is not big difference between strains at 1st ply and the 8th ply this demonstrate that flexible performance of the model having effect up to bottom ply's flexible stretching.

5. CONCLUSIONS

Contact models incorporated into implicit dynamic routine have been simulated successfully which can be used and extend for variety of bodies to a similar system of boundary value problems. In fact it has generalized the models to some extent for variety of cases under variable load intensity. This considerably reduces the complexity and cost of investigation in contact impact studies in practice. The contact duration for this study was small even then the comparison of selected results indicated that material properties have significant effect on the contacting systems. The analysis predicts that quasi-isotropic material systems have indicated more flexibility and strength and could perform better than isotropic material systems in such interacting events.

The approach has demonstrated that some of the contact problems of the similar nature could be solved using implicit dynamic routine. The modeling approach is relatively easier than the explicit dynamic routine. The data results obtained from the solution sets could be utilized to select stronger materials and design improvements as well as to predict failure, damage and fatigue lives of the interacting systems.

REFERENCES

Shtaerman I. J. 1949. Contact Problem of Theory of Elasticity, Moskow.

Timoshenko S. P. and J. M. Goodier. 1951. Theory of elasticity, McGrow Hill, N Y, USA.

Muskhelishvily N. I. 1966. Some Basic Problems of the Mathematical Theory of an Elasticity, Moskow. p. 708.

J.P. Giltrow and J.K. Lancaster. 1970. The role of the counterface in the friction and wear of fibrous resins. Wear. 16(5): 359-374.

Levina Z. M., Reshetov D. N. 1971. Contact Rigidity of Machines, Moskow. p. 264.

Prusov I. A. 1978. Thermal Elastic Non-Isotropic Plate. Minsk. p. 200.

Teply M. I. 1983. The Contact Problems for areas with Circular Boundaries. Lvov. p. 176.

T.M. Tan and C.T. Sun. 1985. Use of static indentation laws in the impact analysis of composite plates. Trans ASME, J Appl Mech. 52 (March). pp. 6-12.

Tan T. M. and Sun C. T. 1985. Use of static indentation laws in the impact analysis of laminated composite plates. J. Appl. Mech. 52: 6-12.

Keer L. M. and Schonberg W. P. 1986. Smooth indentation of a transversely isotropic cantilever beam. Int. J. Solids Struct. 23: 1033-1053.

Cairns D. S. and Lagace P. A. 1987. Thick composite plates subjected to lateral loading. J. Appl. Mech. 54: 611-616.

Johnson K. 1987. Contact Mechanics. Cambridge University Press. p. 510.

Sankar B. V. 1989. Smooth indentation of orthotropic beams. Com. Sci. Tech. 34: 95-111.

Wu E., Chao J. and Yen C. 1993. Smooth contact of orthotropic laminates by rigid cylinders. AIAA J. 31: 1916-1921.

I.H. Choi and C.S. Hong. 1994. New approach for simple prediction of impact force history on composite laminates. AIAA J. 32(10): 2067-2072.

Kovlenko E. W. 1995. Mathematical Modeling of Elastic Bodies. Limited by Cylindrical Surfaces, Friction and Wear. 16(4): 429-438.

Chernets M. 1996. About Method of Calculation of Cylindrical System of Friction. Proc. of Academy of Sciences of Ukraine, NI. pp. 47-50.

S. Abrate. 2001. Modeling impacts on composite structures. Com Struct. 51: 129-138.

A. Al-Mayah K and Soudki. 2004. Effect of sandblasting on interfacial contact behaviour of CFRP-metal couples. J Compos Constr. 9(4): 289-295.

I.H. Choi and C.H. Lim. 2004. Low-velocity impact analysis of composite laminates using linearized contact law. Compos Struct. pp. 125-132.

ABAQUS Standard Users Manual. 2004. Ver 6.7, Hibbitt, Karlsson and Sorenson. Inc., USA.

L.S. Sutherland and C. Guedes Soares. 2005. Impact of low fibre-volume glass reinforced polyester circular plates. Int. J. Impact Eng. 31: 1-23.

Robin Olsson and Soren Nilsson. 2006. Prediction of stresses in composite plates under Hertzian contact load. J Compos Constr. 73: 70-77.

A. Al-Mayah K. Soudki and A. Plumtree. 2006. Effect of sleeve on interfacial CFRP–metal couples. J Ma C Eng, ASCE. 18(6): 825-830.

Tiberkak R, Rechak S, Bachene M. 2006. The dynamic response of composites under low impact. 25th Congress of aero sc, Hamburg, Germany.

K. Alnefaie. 2009. Finite element modeling of composite plates with internal de-lamination Composite Structures. 90(1): 21-27.

Farooq U. and Gregory K. 2009. Finite element modeling and simulation of contact interaction and deformation of carbon fibrous composite beam against rigid indenter. ARPN Journal of Engineering and Applied Sciences. 4(7).